Probing the localized to itinerant behavior of the 4f electron in CeIn_{3−x}Sn_{x} by Gd^{3+} electron spin resonance

E. M. Bittar, C. Adriano, C. Giles, C. Rettori, Z. Fisk, and P. G. Pagliuso

Phys. Rev. B **86**, 125108 — Published 6 September 2012

DOI: 10.1103/PhysRevB.86.125108

Probing the localized to itinerant behavior of the $4f$ electron in $CeIn_{3-x}Sn_x$ by Gd^{3+} electron spin resonance

E. M. Bittar,[1,2,*] C. Adriano,[1] C. Giles,[1] C. Rettori,[1,3] Z. Fisk,[4] and P. G. Pagliuso[1,4]

[1] *Instituto de Física "Gleb Wataghin", UNICAMP, 13083-859, Campinas, SP, Brazil*
[2] *Laboratório Nacional de Luz Síncrotron, C. P. 6192, 13083-970, Campinas, SP, Brazil*
[3] *Centro de Ciências Naturais e Humanas, Universidade Federal do ABC, 09210-170, Santo André, SP, Brazil*
[4] *Department of Physics and Astronomy, University of California Irvine, 92697-4575, Irvine, CA, USA*

(Dated: August 22, 2012)

The $CeIn_{3-x}Sn_x$ cubic heavy fermion system presents an antiferromagnetic transition at $T_N = 10$ K, for $x = 0$, that decreases continuously down to zero upon Sn substitution at a critical concentration of $x_c \approx 0.65$. In the vicinity of $T_N \to 0$ the system shows non-Fermi liquid behavior due to antiferromagnetic critical fluctuations. For high Sn content, $x \gtrsim 2.2$, intermediate valence effects are present. In this work we show that Gd^{3+} doped electron spin resonance (ESR) probes a change in the character of the Ce $4f$ electron, as a function of Sn substitution. The Gd^{3+} ESR results indicate a transition of the Ce $4f$ spin behavior from localized to itinerant. Near the quantum critical point, on the antiferromagnetic side of the magnetic phase diagram, both localized and itinerant behaviors coexist.

PACS numbers: 71.27.+a, 74.40.Kb, 76.30.-v

I. INDRODUCTION

Heavy fermion (HF) systems have shown to the scientific community interesting physical phenomena like antiferromagnetism (AFM), superconductivity (SC)[1] and non-Fermi liquid (NFL) behavior in the vicinity of quantum instabilities.[2] However, the evolution from the high temperature unscreened localized f electrons to itinerant heavy quasiparticles at low temperature is still an open question in condensed matter physics. The description of these HF materials stands on the Kondo lattice model[1] in which there are three important energy scales: the crystalline electric field (CEF) splitting, the characteristic temperature T^* and the single impurity Kondo temperature T_K. The latter is related to the screening of local moments by the conduction electrons due to the Kondo effect. Whereas T^* represents the crossover between a lattice of Kondo impurities to a coherence state where the hybridization becomes a global process. This energy scale is related to the Ruderman–Kittel–Kasuya–Yosida (RKKY) exchange interaction, since it corresponds to the nearest-neighbor intersite coupling, which is mediated by the conduction electrons.[3]

The cubic HF $CeIn_{3-x}Sn_x$ system is an interesting series to study the correlations between T_K and T^*. For $x = 0$ the compound is AFM with $T_N = 10$ K and by Sn substitution, T_N decreases continuously down to zero at a critical concentration $x_c \approx 0.65$.[4,5] This system resembles the behavior of $CeIn_3$ under pressure where a SC state emerges at a critical pressure $P_c \approx 25$ kbar with critical temperature $T_c \approx 0.15$ K as $T_N \to 0$.[6] In the vicinity of P_c and x_c both systems show NFL behavior suggesting that AFM critical fluctuations are present. Recently, the analysis of the magnetic contribution to the specific heat in $CeIn_3$ showed that the magnetic fluctuations in this material are effectively 2D.[7] Indeed, an almost linear dependence of $T_N(x)$ is seen for $CeIn_{3-x}Sn_x$,[5] in contrast to what is predicted by the 3D spin density wave (SDW) theory and it cannot be associated to disorder effects.[8] The reported scenario for the pressure and Sn substitution driven QCP were different. For $CeIn_{3-x}Sn_x$ a SDW description of criticality based on critical exponents analysis of a 3D-AFM was used.[8,9] In the SDW QCP the $4f$ moments are delocalized in the AFM state and no change of the Fermi surface is observed across the QCP.[2] However, in a local class of QCP the $4f$ electrons remain localized in the magnetically ordered phase and there is an abrupt change of the Fermi surface volume at the QCP.[2] For the $CeIn_3$ under pressure a local QCP was proposed due to a Fermi surface volume change observed in de-Haas-van-Alphen measurements.[10] Also, some indication of a first-order quantum phase transition instead of a QCP was reported by nuclear quadrupolar resonance measurements carried out around P_c.[11]

In this work we study the evolution of the Gd^{3+} ESR signal in the $CeIn_{3-x}Sn_x$ system through its QCP. Since Ce^{3+} ESR signal is silent, we chose Gd^{3+} as a probe because it is almost a pure S-state, so its total angular momentum is mainly due to spin, being weakly perturbed by CEF effects. To the best of our knowledge no systematic reports on microscopic studies on the Sn substitution x_c were reported. Our Gd^{3+} ESR results show a change in the character of the Ce $4f$ electron, as a function of Sn substitution, which indicates a transition from localized to itinerant behavior. Near the QCP ($x = 0.5$), on the AFM side of the magnetic phase diagram,[5,8] the Ce $4f$ spin present simultaneously both localized and itinerant characters.

II. EXPERIMENTAL DETAILS

Single crystals of Gd doped $CeIn_{3-x}Sn_x$ are synthesized by the flux-growth technique. Elemen-

tal Ce:Gd:In:Sn are weighted in the ratio 1-y:y:10-(10x/3):10x/3, with a nominal value for y of 0.005 and x = 0, 1.5 and 3. Polycrystalline samples are also grown by arc melting in Argon atmosphere. In this case the reactants ratio used is 1-y:y:3-x:x, with the same nominal value for y and x = 0, 0.5, 0.7, 1.5 and 3. X-ray powder diffraction measurements confirm the cubic $AuCu_3$ (Pm-3m) type structure for all synthesized compounds. The temperature dependence of the magnetic susceptibility, $\chi(T)$, is measured for $2 \leq T \leq 300$ K, after zero field cooling (ZFC). All ESR experiments are performed on a fine powder ($d \leq 38$ μm) in a Bruker ELEXSYS X-band spectrometer (9.4 GHz) with a TE_{102} cavity coupled to a helium-gas-flux temperature controller system for $4.2 \leq T \leq 300$ K. Fine powder of crushed single and polycrystals are used in the ESR experiments in order to increase the ESR signal-to-noise ratio. As a reference compound, Gd doped $LaIn_{3-x}Sn_x$ alloys were also grown and studied.[12]

III. EXPERIMENTAL RESULTS

The actual Sn concentrations are obtained from the cubic lattice parameter which one expects to follow a linear increase (Vegard law)[5] [see Fig. 1(a)]. For $x = 3$ the departure of linear behavior is due to the Ce ions intermediate valence effects for $x \gtrsim 2.2$.[4] The temperature dependence of the magnetic susceptibility $\chi(T)$ for the series of compounds $Ce_{1-y}Gd_yIn_{3-x}Sn_x$, corrected for the core diamagnetism, is shown in Fig. 1(b). From the Curie-Weiss law fitting of the low temperature magnetic susceptibility data, the Gd doping concentration is obtained and its values are shown in Table I.

Figure 2 shows the ESR (X-band) powder spectra, at $T \sim 10$ K, of Gd^{3+} in $CeIn_{3-x}Sn_x$. Except for $x = 0$, the ESR spectra consist of a single Dysonian resonance, consistent with the ESR for localized magnetic moments in a metallic host with a skin depth smaller than the size of the used particles. By fitting the lineshape to the appropriate admixture of absorption and dispersion Lorentzian derivatives, we obtain the g value and linewidth ΔH of the resonances. The solid lines are the best fit to the observed resonances and the obtained g shifts Δg (relative to $g = 1.993(1)$ seen in cubic insulators) are presented in Table I. For Gd^{3+} in $CeIn_3$ the ESR spectrum shows the typical fine-structure features for powder samples,[13] with a main line at $H \sim 3.45$ kOe, associated with the $1/2 \leftrightarrow 1/2$ transition. A previous report in this compound, using the spin Hamiltonian $H = g\mu_B \mathbf{H} \cdot \mathbf{S} + (1/60)b_4(O_4^0 + 5O_4^4) + J_{fs}\mathbf{S}\cdot\mathbf{s}$,[14] extracted the crystal field parameter $b_4 = 90(5)$ Oe.[15] For $Ce_{0.995}Gd_{0.005}In_{2.3}Sn_{0.7}$ a background line is present in the spectrum at $H \sim 3.4$ kOe and for $Ce_{0.99}Gd_{0.01}In_{2.5}Sn_{0.5}$ the ESR spectrum also shows some small contribution of the background. These background contributions are due to extrinsic impurities, with a resonance at $g \sim 2$, present in the cavity or in the cryostat quartz (even without any sample).

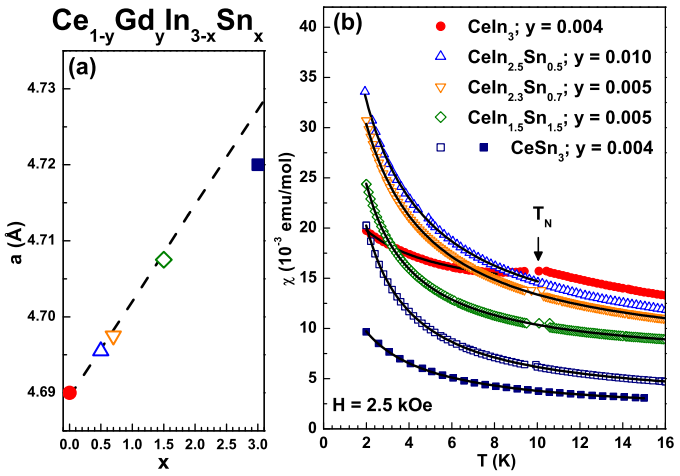

FIG. 1: (color online) Gd^{3+} in $Ce_{1-y}Gd_yIn_{3-x}Sn_x$: (a) cubic lattice parameter a dependance as a function of x. The dashed line represents the Vegard law.[5] For $x = 3$ the departure of linear behavior is due to the Ce ions intermediate valence effects for $x \gtrsim 2.2$.[4] (b) Low temperature dependence of $\chi(T)$ at $H = 2.5$ kOe. The solid lines are the Curie-Weiss fitting. The closed symbols identify the single crystalline samples and the open ones the polycrystals.

The temperature dependence of ΔH is shown in Fig. 3. For all samples there is a range where the width increases linearly with temperature. In this range the linear dependence of the ΔH is fitted to the expression $\Delta H - \Delta H_0 = bT$. The values for ΔH_0 (residual linewidth) and b (linewidth thermal broadening) are presented in Table I and Fig. 4. The relatively high ΔH_0 values for $0 < x < 3$ are probably due to unresolved CEF and disorder introduced by the In-Sn substitution. The ΔH_0 values follow the residual electrical resistivity ρ_0 behavior, since both are dependent on the disorder. One can see that ΔH_0 has the same pattern for $LaIn_{3-x}Sn_x$ [Fig. 4(b)] which follows the ρ_0 dependence (see Fig. 4 of Ref. 16). For $Ce_{0.996}Gd_{0.004}In_3$ only the ΔH temperature dependance of the main line is analyzed. A deviation from the linear dependence of ΔH at low temperature for $x = 1.5$ is related to short range Gd-Gd interaction. Within the accuracy of the measurements, the g and b values are Gd concentration independent for $y < 1.0\%$ (not shown). Therefore, bottleneck and dynamic effects can be disregarded.[17]

Since in this work samples with different Sn content are grown by different methods we show, particularly for $x = 3$ (Fig. 2), that there are no discernable differences in the ESR spectra of grounded single and polycrystalline samples. Hence, for the $CeIn_{3-x}Sn_x$ system, single and polycrystals are undistinguishable from the ESR point of view. However, this is not always the case in most systems and it cannot be established *a priori*. Table I and Fig. 4 do not distinguish single and polycrystalline samples.

The errors bar values presented in Table I and Fig.

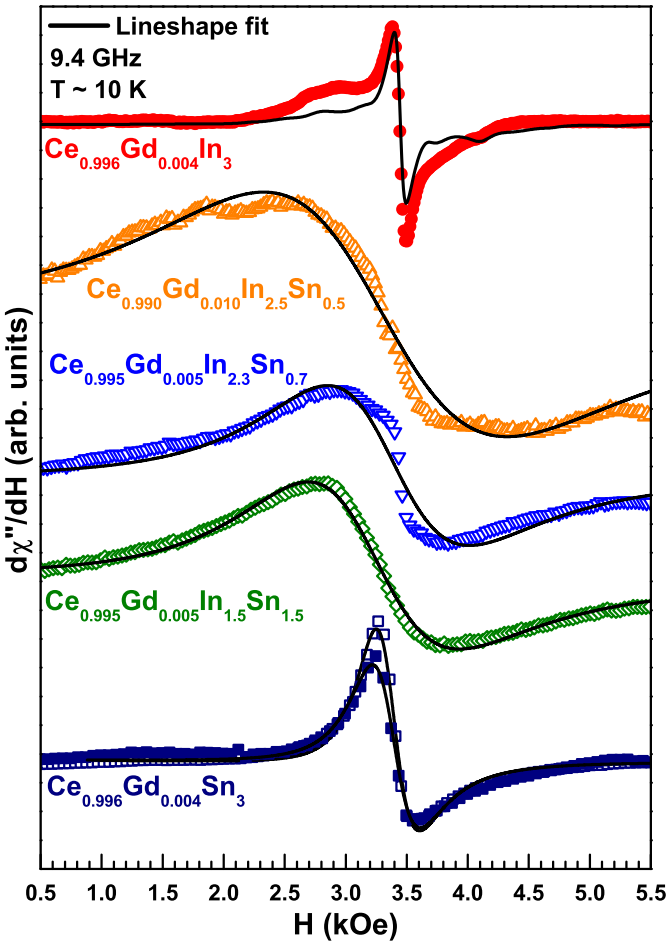

FIG. 2: (color online) Gd^{3+} ESR powder spectra in $Ce_{1-y}Gd_yIn_{3-x}Sn_x$ for $y \sim 0.5\%$, at $T \approx 10$ K, emphasizing the resonance region. The solid lines are the single Dysonian line shape analysis. For $Ce_{0.996}Gd_{0.004}In_3$ it was used the spin Hamiltonian model discussed in Ref. 14 for powder.[15] Background contribution is present for the $x = 0.5$ and $x = 0.7$ samples (see text). The closed symbols identify the single crystalline samples and the open ones the polycrystals.

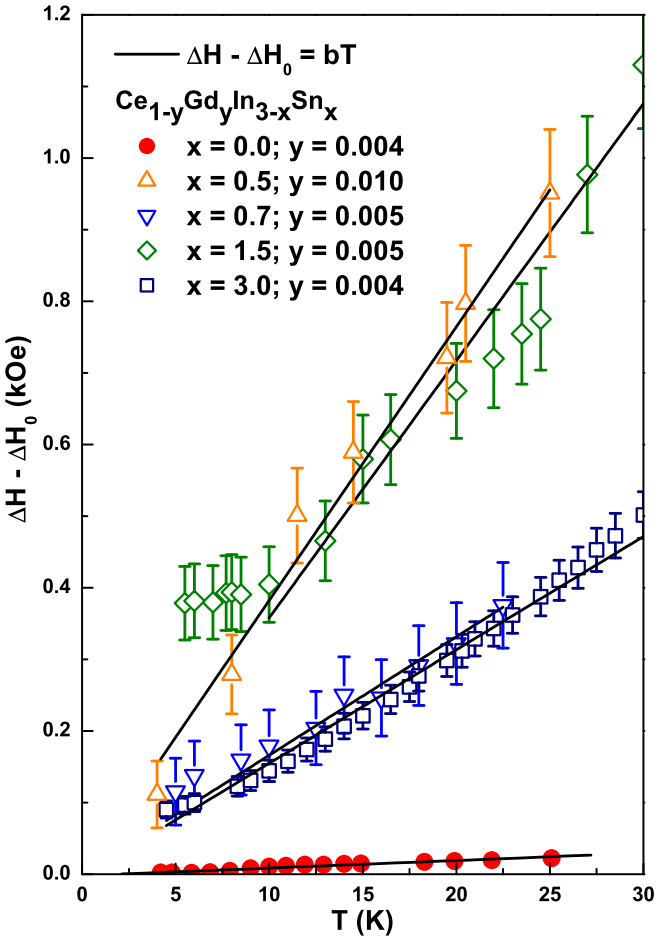

FIG. 3: (color online) Temperature dependence of the Gd^{3+} ESR linewidth in $Ce_{1-y}Gd_yIn_{3-x}Sn_x$. The solid lines are the best fit to $\Delta H - \Delta H_0 = bT$. A deviation from the linear dependence of ΔH at low temperature is seen for $x = 1.5$ which is related to short range Gd-Gd interaction. The closed symbols identify the single crystalline samples and the open ones the polycrystals.

TABLE I: Experimental parameters for Gd^{3+} diluted in $Ce_{1-y}Gd_yIn_{3-x}Sn_x$. The values of γ are taken from Ref. 5.

Gd^{3+} in	Gd y	Δg	ΔH_0 [Oe]	b [Oe/K]	γ [mJ/mol K^2]
$CeIn_3$	0.004	-0.023(5)	120(5)	0.1(1)	130
$CeIn_{2.5}Sn_{0.5}$	0.010	+0.007(10)	825(45)	38(3)	730(50)
$CeIn_{2.3}Sn_{0.7}$	0.005	+0.027(10)	820(25)	15(5)	750(50)
$CeIn_{1.5}Sn_{1.5}$	0.005	+0.140(10)	650(60)	30(5)	250(20)
$CeSn_3$	0.004	+0.027(5)	150(5)	16(1)	73

4 are determined by systematic measurements of different samples for most Sn concentrations and by analyzing the line shape fitting for different field ranges. To exemplify such systematic procedures; Fig. 5 illustrates a line shape analysis for different field range fitting, in this case for the $Ce_{0.990}Gd_{0.010}In_{2.5}Sn_{0.5}$ sample. One can observe that the slope of linewidth thermal broadening [Fig. 5(b)] and the g-value [Fig. 5(c)] of the Gd^{3+} ESR are almost independent of the field range fitting. Also, Fig. 6 exemplifies different samples measurements for $Ce_{0.995}Gd_{0.005}In_{2.3}Sn_{0.7}$. Again, the b and g values [Fig. 6(b)] vary little between samples. Therefore, despite the large linewidth of the Gd^{3+} ESR in $Ce_{1-y}Gd_yIn_{3-x}Sn_x$, that would give rise to large error values, our systematic measurements and fitting procedures allow us to reduce the error and determine the values with higher precision.

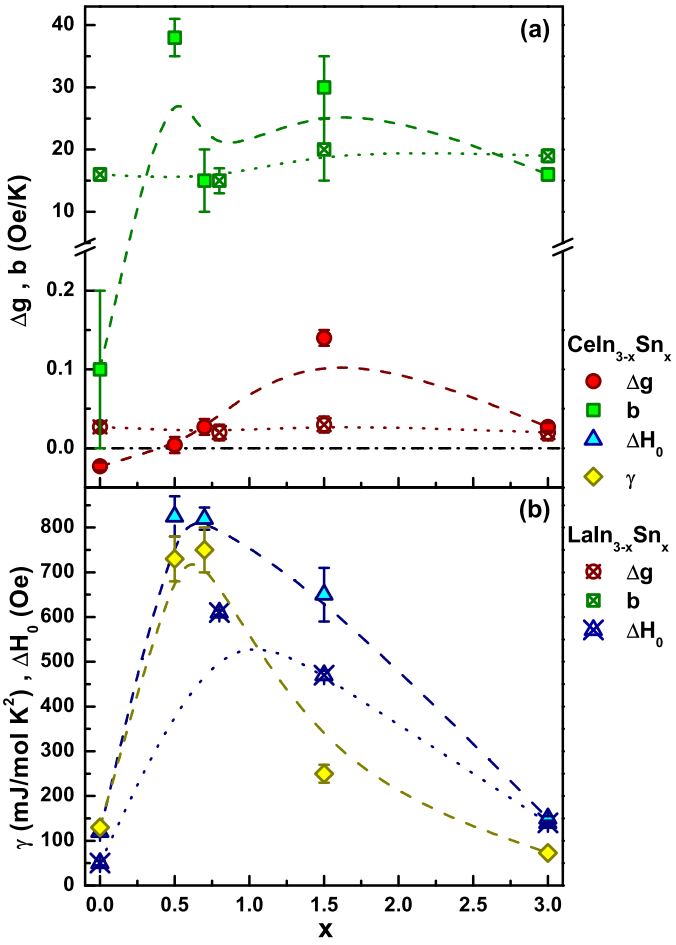

FIG. 4: (color online) Gd^{3+} ESR in $Ce_{1-y}Gd_yIn_{3-x}Sn_x$: (a) linewidth thermal broadening b and g shift evolution. The dash-dot line mark $\Delta g = 0$. (b) Sommerfeld coefficient γ and residual linewidth ΔH_0 evolution. For comparison, the Gd^{3+} ESR in $La_{1-y}Gd_yIn_{3-x}Sn_x$ data are also shown.[12] The dashed and dotted spline lines are guides to the eyes.

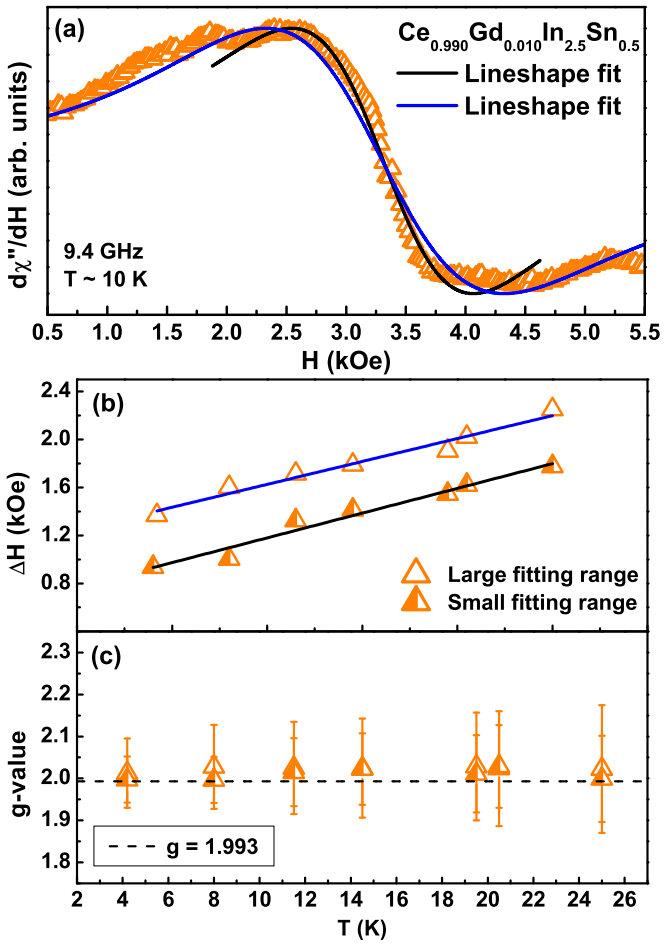

FIG. 5: (color online) (a) Gd^{3+} ESR powder spectra in $Ce_{0.990}Gd_{0.010}In_{2.5}Sn_{0.5}$, at $T \approx 10$ K. The solid lines are the single Dysonian line shape analysis for two different field range fitting. (b) Temperature dependence of the Gd^{3+} ESR linewidth for the two different field ranges shown in (a). The solid lines are the best fit to $\Delta H = \Delta H_0 + bT$. (c) g-value temperature dependence of the Gd^{3+} ESR for the two different field ranges shown in (a). The dashed line is the g-value for Gd^{3+} ESR in insulators.

IV. ANALYSIS

A. Gd^{3+} ESR in metals

In metals, the exchange interaction $J_{fs}(q)\mathbf{S}\cdot\mathbf{s}$ between a Gd^{3+} localized $4f$ electron spin ($\mathbf{S}$) and the conduction electrons spin ($\mathbf{s}$) of the host metal yields an ESR Δg (Knight shift) given by[18]

$$\Delta g = J_{fs}(0)\eta_{F_s}, \qquad (1)$$

where $J_{fs}(0)$ is the effective exchange interaction parameter between the Gd^{3+} $4f$ local moment and the s-like conduction electrons in the absence of conduction electrons momentum transfer ($q = |\mathbf{k} - \mathbf{k}'| = k_F[2(1 - cos\theta_{\mathbf{kk}'})]^{1/2} = 0$).[19] η_{F_s} is the s-like band bare density of states for one spin direction at the Fermi surface.

In addition, the exchange interaction leads to a thermal broadening of ΔH, b (Korringa rate), given by[18]

$$b = \frac{d(\Delta H)}{dT} = \frac{\pi k_B}{g\mu_B} J_{fs}(0)^2 \eta_{F_s}^2, \qquad (2)$$

where the constants k_B, μ_B and g are the Boltzman constant, the Bohr magneton and the Gd^{3+} g value in insulators ($g = 1.993$), respectively. The constant $\pi k_B/g\mu_B$ is 2.34×10^4 Oe/K in CGS units.

Equations 1 and 2 are normally used in the analysis of the ESR data for non interacting and highly diluted rare-earths magnetic moments in intermetallic compounds with appreciable residual resistivity, i.e., large conduction electrons spin-flip scattering (absence of "bottleneck" and "dynamic" effects).[17] Combining the above

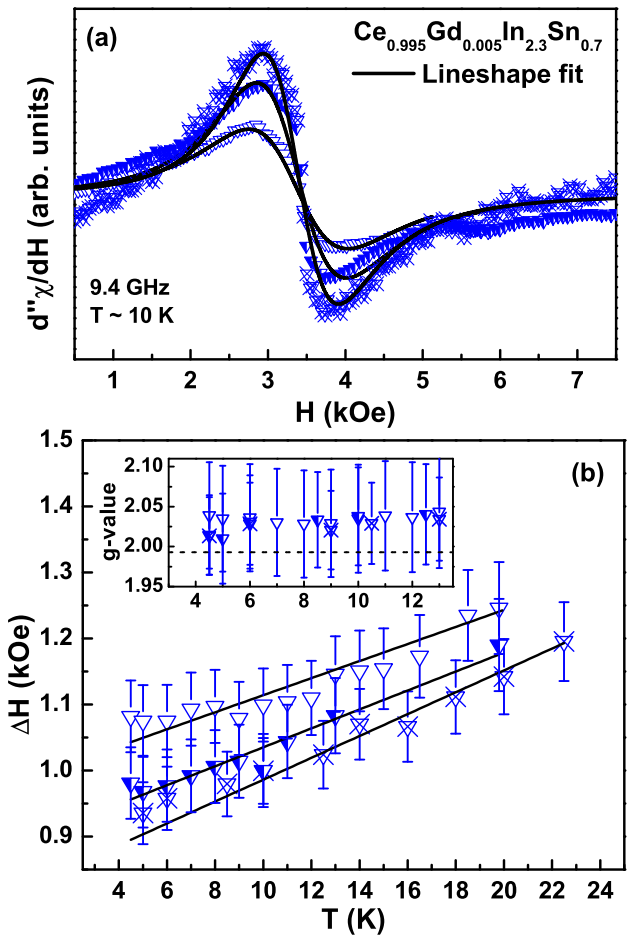

FIG. 6: (color online) (a) Gd^{3+} ESR powder spectra in $Ce_{0.995}Gd_{0.005}In_{2.3}Sn_{0.7}$, at $T \approx 10$ K, for three different samples with same Sn concentration. The solid lines are the single Dysonian line shape analysis. (b) Temperature dependence of the Gd^{3+} ESR linewidth for the three different samples shown in (a). The solid lines are the best fit to $\Delta H = \Delta H_0 + bT$. *Inset*: Low temperature g-value dependence of the Gd^{3+} ESR for the three different samples shown in (a). The dashed line is the g-value for Gd^{3+} ESR in insulators.

equations we can write

$$b = \frac{\pi k_B}{g\mu_B}(\Delta g)^2. \quad (3)$$

When the effective exchange interaction constant is not independent of the momentum transfer ($q \neq 0$), Eq. 2, in this more general case, has to be rewritten as

$$b = \frac{\pi k_B}{g\mu_B}\left\langle J_{fs}^2(q)\right\rangle \eta_{F_s}^2, \quad (4)$$

or alternatively, using Eq. 1

$$b = \frac{\pi k_B}{g\mu_B}\frac{\left\langle J_{fs}^2(q)\right\rangle_F}{J_{fs}^2(0)}\Delta g^2, \quad (5)$$

where $\langle J_{fs}^2(q)\rangle_F$ is the square of the effective exchange interaction parameter in the presence of conduction electrons momentum transfer, averaged over the Fermi surface.[19]

One way to know if the system is momentum transfer dependent is to analyze Eq. 3. If the calculated Korringa rate b_{cal} by the experimental Δg is equal to the experimental Korringa rate b_{exp} ($b_{cal} = b_{exp}$), q dependance can be neglected. However, if $b_{cal} > b_{exp}$ then it cannot. This is because $\langle J_{fs}^2(q)\rangle_F / J_{fs}^2(0) \leq 1$, once $J(q)$ is proportional the Fourier transformation of $J(r)$, which amplitude decreases as function of r. So the average $J(r)$ should be smaller than $J(0)$.

In cases where the conduction band has also d-, p- or f-like electrons, Eqs. 1 and 2 are not valid and must be rewritten, respectively as

$$\begin{aligned}\Delta g &= \Delta g_{fs} + \Delta g_{fd} + \Delta g_{fp} + ... \\ &= J_{fs}(0)\eta_{F_s} + J_{fd}(0)\eta_{F_d} + J_{fp}(0)\eta_{F_p} + ... \quad (6)\end{aligned}$$

and

$$\begin{aligned}b &= \frac{\pi k_B}{g\mu_B}[F_s J_{fs}^2(0)\eta_{F_s}^2 + \\ &+ F_d J_{fd}^2(0)\eta_{F_d}^2 + F_p J_{fp}^2(0)\eta_{F_p}^2 + ...] \quad (7)\end{aligned}$$

where $J_{fs}(0)$, $J_{fd}(0)$ e $J_{fp}(0)$ are the exchange interaction constants between the Gd^{3+} $4f$ spin and the s-, d- and p-like bands, respectively. η_{F_s}, η_{F_d} and η_{F_p} are the bare density of states for one spin direction at the Fermi surface for each respective band. $F_s = 1$, $F_d = 1/5$ and $F_p = 1/3$ are factors associated with the orbital degeneracy of the unsplit (no CEF effects) s, d and p bands at the Fermi level, respectively.[20,21]

Multiband effects enhance the Korringa rate compared to b_{cal}, since the dependance of b is quadratic with the exchange interaction parameters. While for Δg it is linear and depends on the sign and strength of each exchange interaction constant. Therefore, the Δg sign can give valuable information about the interaction between the localized moment and its environment.

B. Gd^{3+} Effective exchange interaction parameter calculations in $CeIn_{3-x}Sn_x$

We now analyze separately the experimental ESR data for each synthesized compound.

1. *Calculation for $x = 0.0$*

In the absence of strong electron-electron exchange interaction and assuming that $\langle J_{fs}^2(q)\rangle_F^{1/2} = J_{fs}(0)$, i.e., the effective exchange interaction is isotropic over the FS, one expects $b \approx 12(5)$ Oe/K from Eq. 3, using the experimental $\Delta g \simeq -23(5) \times 10^{-3}$. This value is much larger than that measured experimentally $b = 0.1(1)$

Oe/K (Fig. 3). Thus, the approximations that the relaxation does not depend on q and that it is due to the contribution of a single conduction s-like band are not adequate. Since Δg is negative, a relaxation via a single s band is not plausible because $J_{fs}(0)$ is atomic-like and positive. Thus, for $\Delta g < 0$, contributions coming from covalent-like (negative) exchange interaction between the Gd^{3+} $4f$-electron and p- or f-bands must be taken into account in the relaxation process (multiband effects).[18] On the other hand, multiple bands would lead to a Korringa rate larger than the one expected from the Δg,[22] contrary to what is observed for Gd^{3+} in $CeIn_3$. Therefore, a strong q dependent effective exchange interaction parameter $J_{fp}(q)$ or $J_{ff}(q)$ is expected in this compound. For $CeIn_3$ the local magnetic moment of Ce is compensated by the conduction electrons sea due to the Kondo effect. However, when Gd^{3+} substitutes the Ce ions there is a strong Coulomb repulsion potential that decreases the local density of states at the Gd^{3+} site, hence decreasing the Korringa rate (Eq. 2 or 4). Theoretical calculations have already shown that the spin relaxation rate of a well-defined magnetic moment in the neighborhood of a fluctuating valence ion decreases in relation to the relaxation rate of a undoped metal.[23] Indeed, a much larger Korringa rate $b = 16(1)$ Oe/K was measured in Gd doped $LaIn_3$.[15] This has also been observed for Gd in $CePd_3$ which presented an ESR ΔH thermal broadening five times smaller than in $LaPd_3$.[24] Besides, the observation of fine-structure features in the spectrum (Fig. 2) even up to room temperature without narrowing effects[18] (not shown) suggests a low local density of states at the Gd^{3+} site. Another consequence of the screening of Ce^{3+} magnetic moment by the conduction electrons is that the Gd^{3+} resonance does not sense the internal field caused by the AFM transition. No change in the relaxation nor in the resonance field is observed below $T_N = 10$ K.

From the considerations above we can assume that the interaction of the Gd^{3+} $4f$ local moment is mainly with the Ce f-like conduction electrons. We then can rewrite Eqs. 1 and 4 respectively as

$$\Delta g = J_{ff}(0)\eta_{F_f} \tag{8}$$

and

$$b = \frac{\pi k_B}{g\mu_B} F_f \left\langle J_{ff}^2(q)\right\rangle_F \eta_{F_f}^2, \tag{9}$$

where $F_f = 1/7$ is associated with the orbital degeneracy of the unsplit f band at the Fermi level.[20,21]

In the free conduction electron gas model, the electronic heat capacity or Sommerfeld coefficient γ is given by

$$\gamma = (2/3)\pi^2 k_B^2 \eta_F \tag{10}$$

and one can obtain, using its experimental value, the bare density of states for one spin direction at the Fermi surface.

For $CeIn_3$ $\gamma^{x=0} = 130$ mJ/(mol K^2),[5] so we get from Eq. 10 $\eta_F^{x=0} = 28(2)$ states/(eV mol spin). Assuming that in this compound the density of states at the Fermi level for the $4f$ electrons $\eta_{F_f}^{x=0}$ is

$$\eta_{F_f}^{x=0} = \eta_F^{x=0} - \eta_F^{LaIn_3},$$

where $\eta_F^{LaIn_3} = 0.8(1)$ states/(eV mol spin) (see Fig. 4 of Ref. 25), we calculate $\eta_{F_f}^{x=0} = 27(2)$ states/(eV mol spin).

Using Eqs. 8 and 9 and experimental values of Δg and b, and $\eta_{F_f}^{x=0} = 27(2)$ states/(eV mol spin), we obtain $J_{ff}(0) = -0.8(1)$ meV and $\langle J_{ff}^2(q)\rangle_F^{1/2} = 0.20(5)$ meV.

2. *Calculation for $x = 0.5$*

By substituting 16.67% of In by Sn, $x = 0.5$, T_N drops to ~ 1.3 K,[5] very close to x_c. We also see Δg going from a relatively large negative to a very small $\simeq 7(10)\times 10^{-3}$ positive value. From Eq. 3 we get $b_{cal} \ll b_{exp}$. It is clear that for $Ce_{0.990}Gd_{0.010}In_{2.50}Sn_{0.50}$ multiband effects are now present.[22] This is expected since Sn substitution lead to the hybridization of the localized Ce^{3+} $4f$ electrons turning them into an itinerant s-like conduction band. So, for $x = 0.5$ the Gd^{3+} resonance relaxes via contribution of the Ce $4f$ itinerant s- and localized f-like bands. In this case, Eqs. 6 and 7 can be rewritten respectively as

$$\Delta g = J_{fs}\eta_{F_f^{it}} + J_{ff}\eta_{F_f^{loc}} \tag{11}$$

and

$$b = \frac{\pi k_B}{g\mu_B}\left[J_{fs}^2\eta_{F_f^{it}}^2 + F_f J_{ff}^2 \eta_{F_f^{loc}}^2\right], \tag{12}$$

where $\eta_{F_f^{it}}$ and $\eta_{F_f^{loc}}$ are the band bare density of states for one spin direction at the Fermi surface for the itinerant- and localized-like $4f$ band, respectively.

From $\gamma^{x=0.5} = 730(50)$ mJ/(mol K^2)[5] and Eq. 10 we get $\eta_F^{x=0.5} = 155(2)$ states/(eV mol spin). Assuming that

$$\eta_{F_f}^{x=0.5} = \eta_F^{x=0.5} - \eta_F^{LaIn_{2.5}Sn_{0.5}},$$

where $\eta_F^{LaIn_{2.5}Sn_{0.5}} = 0.8(1)$ states/(eV mol spin) (see Fig. 4 of Ref. 25), we calculate $\eta_{F_f}^{x=0.5} = 154(2)$ states/(eV mol spin).

Solving the system of three equations below for $\eta_{F_f}^{x=0.5} = 154(2)$ states/(eV mol spin), $\Delta g \simeq 7(10)\times 10^{-3}$, $b = 38(3)$ Oe/K and admitting that $J_{ff}^{x=0.5} = J_{ff}^{x=0} = 0.0008$ eV

$$\eta_{F_f}^{x=0.5} = \eta_{F_f^{it}} + \eta_{F_f^{loc}} = 154,$$

$$\Delta g = J_{fs}\eta_{F_f^{it}} + 0.0008\eta_{F_f^{loc}} = 7\times 10^{-3}$$

and

$$b = 2.34 \times 10^4 \left[J_{fs}^2 \eta_{F_f^{it}}^2 + \frac{1}{7}(0.0008)^2 \eta_{F_f^{loc}}^2 \right] = 38,$$

we obtain $J_{fs}(0) = 0.3(1)$ meV, $\eta_{F_f^{it}} = 115(10)$ states/(eV mol spin) and $\eta_{F_f^{loc}} = 40(5)$ states/(eV mol spin).

So, naively, this result indicates that a weight of 74% of the Ce f-electrons becomes itinerant upon $x = 0.5$ Sn substitution while the other 26% remains localized. One may argue that the multiband effects would be in fact due to the presence of s electrons arising from a weakened Kondo interaction at the Ce^{3+} site or by the addition of new electrons. However, small Sn substitution increases the conduction electrons attractive potential[23] and does not profoundly change the density of states, as seen in $LaIn_{3-x}Sn_x$,[12,25] favoring the interpretation of a delocalization of the Ce f-electrons.

3. *Calculation for $x = 0.7$*

For Gd^{3+} in $CeIn_{2.3}Sn_{0.7}$ the system is in the vicinity of the QCP and Eq. 3 predicts $b_{cal} \approx b_{exp}$. Therefore, we can consider a single s-like conduction band with no q dependance in the analysis of the resonance in this material. Hence, from $\gamma^{x=0.7} = 750(50)$ mJ/(mol K^2)^5 and Eq. 10 we get $\eta_F^{x=0.7} = 160(10)$ states/(eV mol spin). Using Eq. 2 we find $J_{fs}(0) = 0.2(1)$ meV, similar to value encountered for $x = 0.5$.

4. *Calculation for $x = 1.5$*

The Δg value observed experimentally gives $b_{cal} \gg b_{exp}$ by Eq. 3. So, in this case q dependance is present and $\langle J_{fs}^2(q) \rangle_F^{1/2} \neq J_{fs}(0)$. From $\gamma^{x=1.5} = 250(20)$ mJ/(mol K^2)^5 and Eq. 10 we get $\eta_F^{x=1.5} = 53(4)$ states/(eV mol spin). Using Eqs. 1 and 4 we calculate $J_{fs}(0) = 2.6(2)$ meV and $\langle J_{fs}^2(q) \rangle_F^{1/2} = 0.7(1)$ meV, respectively.

5. *Calculation for $x = 3.0$*

From Eq. 3 we get $b_{cal} \approx b_{exp}$, i.e., multiband and q dependance effects of the exchange interaction may be neglected. Thus, from $\gamma^{x=3} = 73$ mJ/(mol K^2)^5 and Eq. 10 we get $\eta_F^{x=3} = 16(1)$ states/(eV mol spin). Using Eq. 2 we find $J_{fs}(0) = 1.7(1)$ meV.

C. Derived effective exchange interaction parameters summary

The derived effective exchange interaction parameters from the analysis above are summarized in Table II. Due to the suppositions and approximations considered in the calculations, the numerical values must be taken with care. However, it does not invalidate the qualitative microscopic description probed by ESR.

TABLE II: Derived effective exchange interaction parameters for Gd^{3+} diluted in $CeIn_{3-x}Sn_x$.

Gd^{3+} in	$J_{fs}(0)$ [meV]	$\langle J_{fs}^2(q) \rangle_F^{1/2}$ [meV]	$\lvert J_{ff}(0) \rvert$ [meV]	$\langle J_{ff}^2(q) \rangle_F^{1/2}$ [meV]
$CeIn_3$			0.8(1)	0.20(5)
$CeIn_{2.5}Sn_{0.5}$	0.3(1)		0.8(1)	
$CeIn_{2.3}Sn_{0.7}$	0.2(1)			
$CeIn_{1.5}Sn_{1.5}$	2.6(2)	0.7(1)		
$CeSn_3$	1.7(1)			

V. DISCUSSION

The nonmagnetic analog $LaIn_{3-x}Sn_x$ system is superconducting and shows Pauli paramagnetism in the normal sate.[25] Gd^{3+} doped ESR measurements in these compounds showed that the g shift and Korringa rate are not strongly changed by Sn substitution [see Fig. 4(a)].[12] The Gd^{3+} relaxation in these alloys is always via a single s-like conduction band and J_{fs} is q independent, slightly decreasing with increasing x (Fig. 7).[12]

For the $CeIn_{3-x}Sn_x$ compounds the evolution of the Gd^{3+} ESR with Sn substitution is not as straightforward as in $LaIn_{3-x}Sn_x$. The b and Δg values profoundly change as a function of x [Fig. 4(a)]. For $CeIn_3$, as we have seen, there is no exchange interaction between Gd^{3+} and the s-like conduction electrons. This is due to the Kondo effect that creates an attractive potential for these s-like conduction electrons at the Ce sites, reducing its density at the Gd site. In this case, the Gd^{3+} ESR relaxes only via a f-like localized band. This attests that the Ce $4f$ electrons in $CeIn_3$ are strongly localized under high Kondo screening, which also prevents the Gd^{3+} resonance from sensing the AFM transition below $T_N = 10$ K.

As the system approaches the QCP ($x = 0.5$), but still presenting AFM order, we observe the appearance of multiband effects in the resonance which are related to the delocalization of the $4f$ electrons, induced by the Sn substitution, giving rise to a s-like band. For this alloy the Ce $4f$ electrons coexist as localized and itinerant.In the vicinity of the QCP ($x = 0.7$), on the nonmagnetic side of the phase diagram, the resonance assumes a character where the relaxation is via a single s-like band. The effective exchange interaction parameter $J_{fs}(0)$ in this compound is, within experimental errors, the same as at $x = 0.5$, but no local f-like electrons are probed by the Gd^{3+}, only the itinerants.

Further increase in the Sn substitution does not alter the Gd^{3+} relaxation process, which remains being

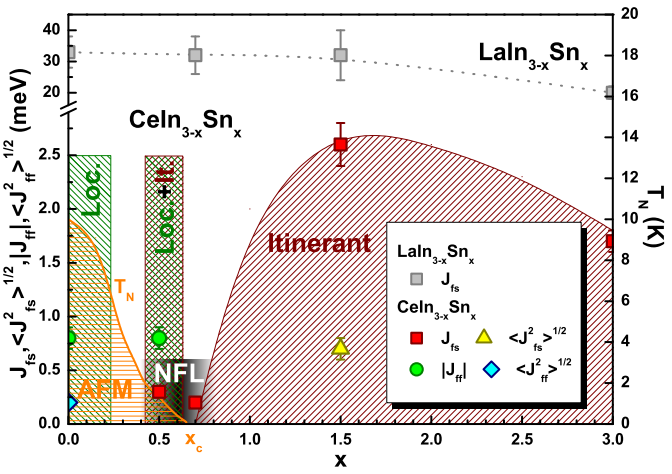

FIG. 7: (color online) Effective exchange interaction parameter evolution as a function of Sn substitution. The data for the $LaIn_{3-x}Sn_x$ compounds are taken from Ref. 12. The AFM temperature transition T_N evolution and the non-Fermi liquid (NFL) region in the vicinity of the critical Sn concentration x_c are also seen.[5] For $CeIn_{3-x}Sn_x$ one can identify the presence of only the localized (Loc.) spin behavior for $x = 0$ and the itinerant (It.) character for $x \geq 0.7$, since only a single band effective exchange interaction is probed in each case. At $x = 0.5$, near the quantum critical point, Gd^{3+} ESR probes both localized and itinerant components of the Ce $4f$ electron. The shaded areas and spline lines are guides to the eyes.

via a single s-like conduction band. For $x = 1.5$ the exchange interaction is q dependent, indicating that it is not isotropic over the Fermi surface and this dependance might be related with an anisotropy observed in the s-f hybridization for $CeIn_1Sn_2$.[26] In $CeSn_3$ the $J_{fs}(0)$ value decreases slightly compared to $CeIn_{1.5}Sn_{1.5}$, probably due to intermediate valence effects and/or lattice expansion. Thus, once the system crosses the QCP the hybridization of the localized $4f$ electrons with the conduction band becomes a global process and it behaves only as itinerant.

Fig. 7 summarizes qualitatively this discussion of the Gd^{3+} ESR evolution in the $CeIn_{3-x}Sn_x$ materials.

VI. CONCLUSIONS

For $CeIn_{3-x}Sn_x$, our conclusions are not drawn solely based on the values of the extracted or derived parameters, as a function of Sn concentration, but mostly on the fact that one cannot analyze in the same way the Gd^{3+} ESR of each sample. When comparing the $LaIn_{3-x}Sn_x$[12] and $CeIn_{3-x}Sn_x$ systems, one can immediately realize that the evolution by substituting In by Sn is dramatically different. While for the La based compounds only a slight change of the $J_{fs}(0)$ value is observed, for the HF one, the Gd^{3+} effective exchange parameter alters significantly depending on the x value. However, the only difference between these systems is an addition of a $4f$ electron. So, the discrepancy in the evolution behavior must come from the physics of this extra $4f$ electron. For the $x = 0$ end member this additional electron is localized and highly screened by the conduction electron sea and thus, Gd^{3+} ESR only probes a f-like localized band. Whereas for the other end member, $x = 3$, no local magnetism occurs and the compound can be described as a HF Landau Fermi Liquid, where the Gd^{3+} resonance relaxes only via a single s-like itinerant band. On the other hand, in between, specifically for $x = 0.5$, we observe a multiband effects on the ESR data, i.e., contribution of localized and itinerant bands that are originated by the same Ce extra $4f$ electron. Therefore, we argue that the microscopic evolution of the $4f$ electron in the $CeIn_{3-x}Sn_x$ system, as a function of Sn substitution, can be understood as a transition from localized to itinerant. Where the localized character exists only on the AFM phase and dies out at the QCP, while the itinerant behavior can even coexist in the AFM state.

From the ESR results we observe that there are still some local moments very close to the QCP on the AFM state ($x = 0.5$) and none in its vicinity on the nonmagnetic side ($x = 0.7$) of the phase diagram. However, from our data, it is difficult to assert on whether the QCP in $CeIn_{3-x}Sn_x$ is of the itinerant or localized scenario and further ESR experiments in samples with different Sn content are needed to clarify this issue.

VII. SUMMARY

In summary, our ESR results microscopically show that for the $CeIn_{3-x}Sn_x$ system the AFM end member has only highly screened local moments whereas for the nonmagnetic samples just itinerants bands are probed. For $x = 0.5$, in the vicinity of the QCP, on the AFM side of the magnetic phase diagram, the $4f$ electrons has a dual character being at the same time localized and itinerant, giving rise to multiband effects.

Acknowledgments

We thank J. C. B. Monteiro and F. C. G. Gandra for the help with the polycrystalline samples. This work was supported by FAPESP [Grant Nos. 06/55347-1 and 06/60440-0], CNPq, FINEP and CAPES (Brazil) and NSF [Grant No. NSF-DMR-0801253] (USA).

* Electronic address: eduardo.bittar@lnls.br

[1] G. R. Stewart, Rev. Mod. Phys. **56**, 755 (1984).

[2] H. v. Löhneysen, A. Rosch, M. Vojta, and P. Wölfle, Rev. Mod. Phys. **79**, 1015 (2007).

[3] S. Nakatsuji, S. Yeo, L. Balicas, Z. Fisk, P. Schlottmann, P. G. Pagliuso, N. O. Moreno, J. L. Sarrao, and J. D. Thompson, Phys. Rev. Lett. **89**, 106402 (2002).

[4] J.M. Lawrence, Phys. Rev. B **20**, 3770 (1979).

[5] P. Pedrazzini, M. G. Berisso, N. Caroca-Canales, M. Deppe, C. Geibel, and J. G. Sereni, Eur. Phys. J. B **38**, 445 (2004).

[6] N. D. Mathur, F. M. Grosche, S. R. Julian, I. R. Walker, D. M. Freye, R. K. W. Haselwimmer, and G. G. Lonzarich, Nature **394**, 39 (1998).

[7] N. Berry, E. M. Bittar, C. Capan, P. G. Pagliuso, and Z. Fisk, Phys. Rev. B **81**, 174413 (2010).

[8] R. Küchler, P. Gegenwart, J. Custers, O. Stockert, N. Caroca-Canales, C. Geibel, J. G. Sereni, and F. Steglich, Phys. Rev. Lett. **96**, 256403 (2006).

[9] A. V. Silhanek, T. Ebihara, N. Harrison, M. Jaime, K. Tezuka, V. Fanelli, and C. D. Batista, Phys. Rev. Lett. **96**, 206401 (2006).

[10] R. Settai *et al.*, J. Phys. Soc. Jpn. **74**, 3016 (2005).

[11] S. Kawasaki, M. Yashima, Y. Kitaoka, K. Takeda, K. Shimizu, Y. Oishi, M. Takata, T. C. Kobayashi, H. Harima, S. Araki, H. Shishido, R. Settai, and Y. Ōnuki, Phys. Rev. B **77**, 064508 (2008).

[12] E. M. Bittar, C. Adriano, C. Giles, C. Rettori, Z. Fisk, and P. G. Pagliuso, J. Phys.: Condens. Matter **23**, 455701 (2011).

[13] T. Gambke, B. Elschner, and L. L. Hirst, Phys. Rev. Lett. **40**, 1290 (1978).

[14] J. G. S. Duque, R. R. Urbano, P. A. Venegas, P. G. Pagliuso, C. Rettori, Z. Fisk, and S. B. Oseroff, Phys. Rev. B **76**, 125114 (2007) and references therein.

[15] E. M. Bittar, J. G. S. Duque, P. A. Venegas, C. Rettori, and P. G. Pagliuso, Physica B **404**, 2995 (2009).

[16] W. D. Grobman, Phys. Rev. B **5**, 2924 (1972).

[17] C. Rettori, H. M. Kim, E. P. Chock, and D. Davidov, Phys. Rev. B **10**, 1826 (1974).

[18] S. E. Barnes, Adv. Phys. **30**, 801 (1981).

[19] D. Davidov, K. Maki, R. Orbach, C. Rettori, and E.P. Chock, Solid State Commun. **12**, 621 (1973).

[20] G. E. Barberis, D. Davidov, J. P. Donoso, C. Rettori, J. F. Suassuna, and H. D. Dokter, Phys. Rev. B **19**, 5495 (1979); A. Troper and A. A. Gomes, *ibid.* **34**, 6487 (1986).

[21] Y. Yafet and V. Jaccarino, Phys. Rev. **133**, A1630 (1964).

[22] R. R. Urbano, E. M. Bittar, M. A. Pires, L. Mendonça Ferreira, L. Bufaiçal, C. Rettori, P. G. Pagliuso, B. Magill, S. B. Oseroff, J. D. Thompson, and J. L. Sarrao, Phys. Rev. B **75**, 045107 (2007).

[23] J. W. M. Pinto and H. O. Frota, Phys. Rev. B **64**, 092404 (2001); A. Ghosh, M. S. Gusmão, and H. O. Frota, Eur. Phys. J. B *in press*.

[24] T. Gambke and B. Elschner, J. de Phys. Colloques **40**, C5-331 (1979).

[25] A. M. Toxen, R. J. Gambino, and L. B. Welsh, Phys. Rev. B **8**, 90 (1973).

[26] A. P. Murani, A. Severing, M. Enderle, P. Steffens, and D. Richard, Phys. Rev. Lett. **101**, 206405 (2008).